Report

Current Biology

Ultra-black Camouflage in Deep-Sea Fishes

Highlights

- Reflected bioluminescence can reveal deep-sea animals to predators or prey
- At least 16 species of deep-sea fishes have ultra-black skin (<0.5% reflectance)
- Fish achieve low reflectance using a continuous layer of melanosomes in the skin
- The size and shape of these melanosomes are optimal for reducing reflectance

Authors

Alexander L. Davis, Kate N. Thomas, Freya E. Goetz, Bruce H. Robison, Sönke Johnsen, Karen J. Osborn

Correspondence

alexander96davis@gmail.com

In Brief

Davis et al. investigate the distribution and production of ultra-black camouflage in deep-sea fishes. These fishes have a continuous layer of melanosomes in the dermis that are optimized in size and shape to allow them to reflect <0.5% of light. Sighting distance models suggest low reflectance reduces predator sighting distance up to 6-fold.

Davis et al., 2020, Current Biology *30*, 3470–3476
September 7, 2020
https://doi.org/10.1016/j.cub.2020.06.044

CellPress

CellPress

Current Biology

Report

Ultra-black Camouflage in Deep-Sea Fishes

Alexander L. Davis,[1,6,*] Kate N. Thomas,[2] Freya E. Goetz,[3] Bruce H. Robison,[4] Sönke Johnsen,[1,5] and Karen J. Osborn[3,4,5]
[1]Department of Biology, Duke University, Durham, NC 27708, USA
[2]Department of Life Sciences, The Natural History Museum, London SW7 5BD, UK
[3]Department of Invertebrate Zoology, Smithsonian National Museum of Natural History, Washington, DC 20013, USA
[4]Monterey Bay Aquarium Research Institute, Moss Landing, CA 95039, USA
[5]Senior author
[6]Lead Contact
*Correspondence: alexander96davis@gmail.com
https://doi.org/10.1016/j.cub.2020.06.044

SUMMARY

At oceanic depths >200 m, there is little ambient sunlight, but bioluminescent organisms provide another light source that can reveal animals to visual predators and prey [1–4]. Transparency and mirrored surfaces—common camouflage strategies under the diffuse solar illumination of shallower waters—are conspicuous when illuminated by directed bioluminescent sources due to reflection from the body surface [5, 6]. Pigmentation allows animals to absorb light from bioluminescent sources, rendering them visually undetectable against the dark background of the deep sea [5]. We present evidence suggesting pressure to reduce reflected bioluminescence led to the evolution of ultra-black skin (reflectance <0.5%) in 16 species of deep-sea fishes across seven distantly related orders. Histological data suggest this low reflectance is mediated by a continuous layer of densely packed melanosomes in the exterior-most layer of the dermis [7, 8] and that this layer lacks the unpigmented gaps between pigment cells found in other darkly colored fishes [9–13]. Using finite-difference, time-domain modeling and comparisons with melanosomes found in other ectothermic vertebrates [11, 13–21], we find the melanosomes making up the layer in these ultra-black species are optimized in size and shape to minimize reflectance. Low reflectance results from melanosomes scattering light within the layer, increasing the optical path length and therefore light absorption by the melanin. By reducing reflectance, ultra-black fish can reduce the sighting distance of visual predators more than 6-fold compared to fish with 2% reflectance. This biological example of efficient light absorption via a simple architecture of strongly absorbing and highly scattering particles may inspire new ultra-black materials.

RESULTS AND DISCUSSION

Open-ocean animals exhibit several strategies for hiding from visual predators: among them are mirrored surfaces, transparency, counterillumination, and pigmentation [22]. Transparency and mirror-based camouflage are most effective under diffuse ambient lighting and are thus more common in near-surface waters [5, 23]. Counterillumination operates by replacing the downwelling light blocked by the body from viewers below with light emitted by banks of ventral photophores [1, 24–26] but does not protect organisms from predators viewing laterally or from above. Pigmentation is common in pelagic animals at all depths; however, in the mesopelagic and bathypelagic realms, where there is little solar illumination and organisms must contend with light from bioluminescent sources, pigmentation may be a particularly effective camouflage strategy [1–5]. In the darkness of the lower mesopelagic and bathypelagic zones, reflecting even a small percentage of bioluminescence may reveal an animal to visual predators or potential prey. Mirrored surfaces and white animals reflect >50% of light, and although transparent animals reflect >0.4%, this is potentially enough to allow detection where vision is often tuned to detect just a few photons [6, 27, 28]. Because of the predicted ineffectiveness of these other camouflage methods against bioluminescence, we hypothesized that selective pressure to limit reflected light would lead to the evolution of pigmented body surfaces with near-zero reflectance in deep-sea animals. Here, we focus on deep-sea fishes, which are often black, instead of deep-sea invertebrates, which are typically red but appear black due to the lack of red light in the deep sea [5], because black surfaces have the potential to inspire the design of synthetic ultra-black materials.

Reflectances of Ultra-black Fishes

To test for ultra-black coloration (average reflectance <0.5% across the visible spectrum) as opposed to black coloration (reflectance >0.5%) in deep-sea fishes, we collected specimens via Tucker trawl [29] on two research cruises, one in the Gulf of Mexico and the other in Monterey Bay, CA. Fishes were kept in chilled seawater (4°C–6°C) between capture and reflectance measurement. We used a back-reflectance probe calibrated to a 2% diffuse reflectance standard to measure the reflectance at perpendicular incidence from the blackest undamaged patches of skin. In total, we measured the skin reflectance from 18 species of black fish representing seven taxonomic orders (n = 39

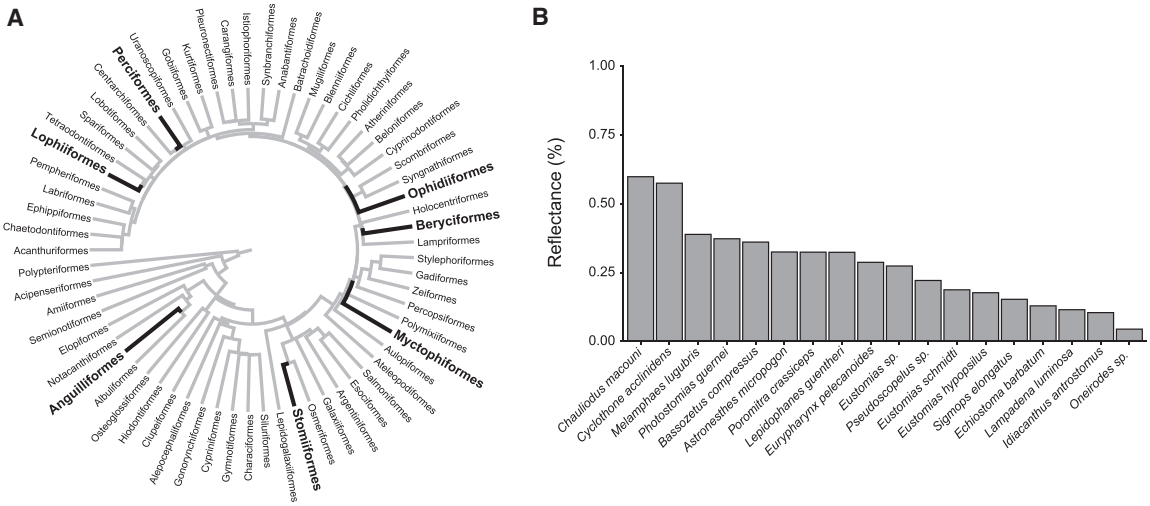

Figure 1. Phylogenetic Distribution and Reflectance of Ultra-black, Deep-Sea Fishes

(A) Order-level phylogeny of Actinopterygii from TimeTree [35] with red branches indicating the presence of at least one ultra-black species from our sampling in that order. These orders are separated by many containing fishes that are primarily colorful or silvery, suggesting that low reflectance may have evolved multiple times independently.

(B) The median reflectance at 480 nm of 18 species of ultra-black, deep-sea fishes. Of these ultra-black fishes, 16 have median reflectances <0.5% (minimum 0.044%; *Oneirodes* sp.). *Chauliodus macouni* and *Cyclothone acclinidens* were included despite having median reflectances above our defined threshold for ultra-black because a substantial number of reflectance measurements for each species were <0.5% at 480 nm.

See also Table S1 and Figure S1.

specimens total; Table S1; Figure S1). Of these, 16 species exhibited reflectances less than 0.5% at 480 nm (approximately the peak wavelength of deep-sea ambient sunlight and most oceanic bioluminescence) [30], and the remaining two species (*Chauliodus macouni* and *Cyclothone acclinidens*) reflected less than 0.6% at 480 nm (Figure 1). The mean reflectance across the visible spectrum for each species ranged from 0.051% to 1.04%, with 14 species exhibiting broadband reflectance <0.5%. This low reflectance puts deep-sea fishes on par with the blackest known animals, with the species exhibiting the lowest reflectance measured here (*Oneirodes* sp.; 0.044% at 480 nm; 0.051% average reflectance from 350 to 700 nm), surpassing the darkness of ultra-black butterflies (0.06%–0.5% reflectance) and equaling the blackest birds of paradise (0.05%–0.31% reflectance) [31–33]. By comparison, man-made materials, such as black paper, reflect ~10% of incident light, and the blackest synthetic materials, manufactured from vertically aligned carbon nanotubes, reflect 0.045% of light [34].

Except for *Cyclothone acclinidens*, *Chauliodus macouni*, and *Sigmops elongatus*, we found ultra-black skin covering most of the body, suggesting that it functions to reduce reflection from bioluminescence (including the searchlights of predators and defensive reactions of prey) [3]. Generally, the fishes studied here are intermediate in size; therefore, pressure to hide from both potential predators and prey could be important forces driving the evolution of ultra-black skin. We also hypothesize that ultra-black skin in ambush predators that use lures, such as *Oneirodes* sp., *Eustomias* spp., and *Astronesthes micropogon*, serves to reduce reflection from their own bioluminescent lures. In species such as *S. elongatum* and *C. macouni*, ultra-black skin is found above and below a mirrored stripe running the length of the body, suggesting that, for areas of the body with high curvature, where mirror-based camouflage may be less effective, ultra-black may provide a substitute. Finally, ultra-black skin is found only around the gut in species like *C. acclinidens* and may be used to conceal light emitted from recently consumed bioluminescent prey [1, 36, 37].

Close-Packed Melanosome Layers Mediate Extremely Low Reflectance in Ultra-black Fishes

We used a combination of scanning electron microscopy (SEM), transmission electron microscopy (TEM), and light microscopy to assess the skin ultrastructure underlying ultra-black coloration (Figures 2 and S2). We analyzed skin samples from nine species of ultra-black fishes from six distantly related orders and six black species without reflectance data including species from one additional order. In the nine ultra-black species, we found a layer of close-packed melanosomes (organelles that contain melanin) that extends continuously with few, if any, unpigmented gaps and no clear separation into individual melanophores (pigment cells containing melanosomes; Figures 2 and S2). Such continuity in the melanosome layer contrasts with many darkly pigmented (but not ultra-black) fishes, where melanophores in the skin are separated by unpigmented gaps occupied by collagen and other cells [9–12, 38]. The average thickness of the melanosome layer in the ultra-black species for which we could acquire light microscopy data was 7.9 μm (n = 6 species) with a range of 2.8 ± 1.2 μm (*Eustomias schmidti*) to 14.3 ± 8.7 μm (*Oneirodes* sp.; simulated below). We found a similar layer in the six species (Figure S2; Table S1) for which we did not have the opportunity to measure reflectance, suggesting that this skin morphology may be important for reducing reflectance in other orders.

Melanophores are found in various fishes within various dermal strata [7, 9, 11, 14, 38–40] and occasionally in the epidermis

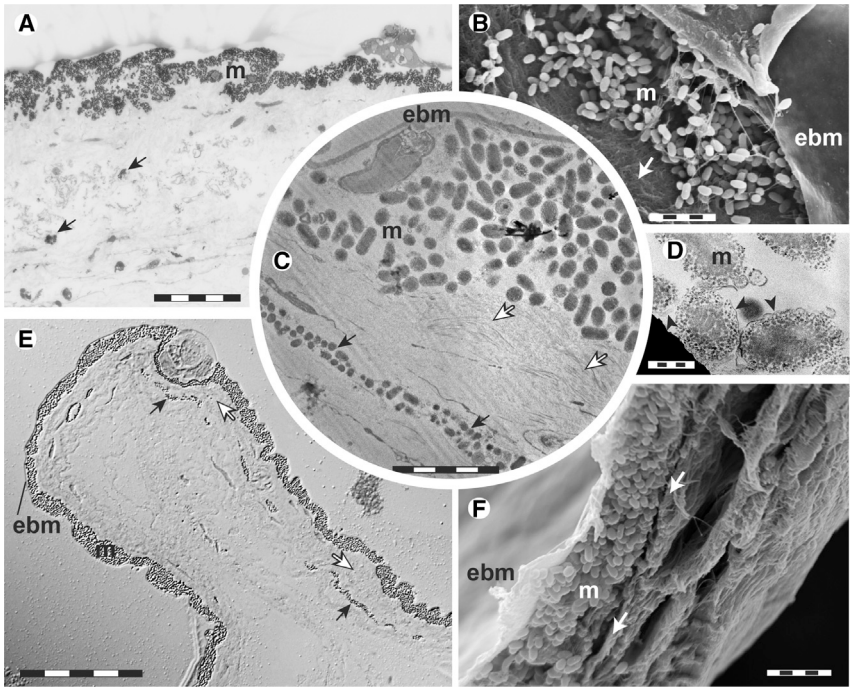

Figure 2. Skin Ultrastructure and Melanosome Geometry

Histology and TEM of the skin of *Oneirodes* sp. (A) and *Idiacanthus antrostomas* (B–F) reveal a continuous layer of melanosomes (m) immediately beneath the epidermal basement membrane (ebm). Melanosomes are membrane-bound organelles (black arrowheads). Melanophores (black arrows) are seen beneath the stratum compactum (white arrows). Scale bars, (A and E) 50 μm; (B, C, and F) 5 μm; (D) 0.5 μm. See also Figure S2.

[10, 41]. The melanosome layers observed here were consistently located immediately between the epidermal basement membrane and the stratum spongiosum (Figures 2 and S2), a loosely organized collagenous layer of the dermis [39]. Species exhibited various amounts of randomly oriented collagen fibers typical of the stratum spongiosum around and between melanosomes (Figures 2B, S2A, S2B, S2E, S2H, and S2K), but none exhibited the expected layer of collagen typically surrounding and supporting pigment cells in fishes [7, 14, 40, 41]. Several species had a thick stratum compactum internal to the melanosome layer (Figures 2C, 2E, 2F, S2N, and S2O), as well as various other layers of continuous and discontinuous melanophores below the stratum compactum (Figures 2A, 2C, 2E, S2L, S2M, and S2O).

We used SEM images to measure melanosome length and width to calculate individual melanosome size (as sphere equivalent diameter—the diameter of a sphere with a volume equivalent to the melanosome—hereafter SED) and aspect ratio (the ratio of the length to width) in seven species (*Bassozetus compressus*, *Echiostoma barbatum*, *Eurypharynx pelecanoides*, *Idiacanthus antrostomus*, *Lampadena luminosa*, *Oneirodes* sp., and *Pseudoscopelus* sp.; Table S1). We chose these parameters because both the size and aspect ratio of an ellipsoid change the amount and direction of scattering and thus have the potential to affect the reflectance of melanosome layers. Melanosome SED ranged from 440 ± 50 nm (*E. pelecanoides*) to 785 ± 120 nm (*E. barbatum*) with a mean across all species of 612 nm (n = 7; Figure 3). The mean melanosome aspect ratio was 2.1 and species averages ranged from 1.5 ± 0.3 (*E. pelecanoides*) to 2.9 ± 0.6 (*Oneirodes* sp.; Figure 3). Compared to other ectothermic vertebrates, ultra-black fish had larger (higher SED) melanosomes, particularly for a given aspect ratio [11, 13–21]. We restricted our comparison to ectothermic vertebrates because birds and mammals have convergently evolved changes in the melanocortin system related to metabolism that affects melanosome geometry [17]. The large melanosome size in ultra-black deep-sea fishes compared to other vertebrates may affect the absorption of light in the melanosome layer.

Size and Aspect Ratio of Melanosomes Combine to Produce Low Reflectance

After identifying the skin ultrastructure responsible for producing ultra-black coloration in these deep-sea fishes, we used mathematical models to determine the mechanism by which the melanosome layer produced low reflectance. To do this, we used 3-dimensional finite-difference time-domain (FDTD) optical simulations of random close-packed aggregations of melanosomes. Given the substantial interspecific variation in aspect ratio and SED observed with SEM, we chose to simulate layers of melanosomes with 169 different combinations of SED and aspect ratio (13 × 13). Thus, in our models, aspect ratio varied from 1.0 to 4.0 in increments of 0.25, and SED varied from 100 nm to 3,000 nm in increments of 100 nm for SED $\leq$ 1,000 nm and 500 nm for SED > 1,000 nm. Simulations of 5 × 5 × 5 μm skin sections backed by a 100% broadband reflector, mimicking the white muscle and collagen beneath the melanosomes, revealed that both size and aspect ratio had significant impacts on reflectance (Figure 3A). Layers containing melanosomes with an aspect ratio near 2.0 and SED of 600–800 nm have the lowest reflectance. As SED increases above 1,000 nm, modeled reflectance of the melanosome layer increases sharply from <1.5% at SED = 600 nm to >10% at SED = 2,000 nm. Similarly, reflectance increases in layers with small melanosomes (SED < 400 nm), particularly when the melanosomes have low aspect ratios. Based on these models, we hypothesize that the melanosome layer produces low reflectance by scattering light sideways within the layer, thus increasing the path length for light absorption.

Comparing the measured melanosome geometry to the model results reveals that the melanosomes in ultra-black fish are well optimized for producing low reflectance, suggesting both the relative accuracy of the model and possible selection for the melanosome geometry observed (Figure 3A). This contrasts with the melanosome geometry in the skin of 50 other species of ectothermic vertebrates, which produce black and brown coloration and have SEDs between 270 nm and 550 nm and aspect ratios between 1.26 and 2.24 [11, 13–21]. Our modeling

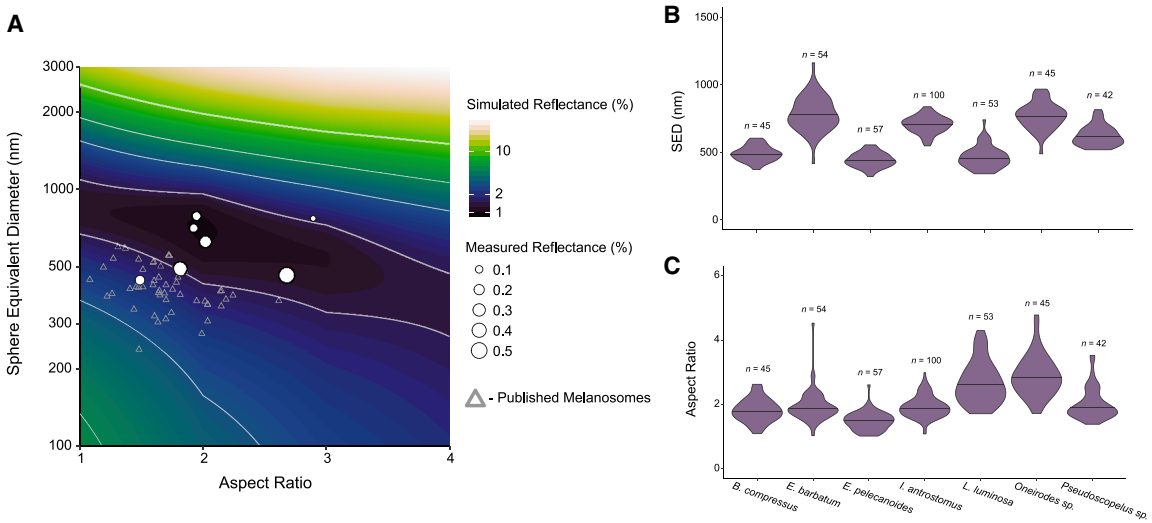

Figure 3. Finite-Difference Time-Domain Modeling of Close-Packed Melanosomes

(A) FDTD simulations of the reflectance from 350–700 nm of close-packed melanosomes with 169 unique combinations of aspect ratio and size reveal that the melanosome geometries of ultra-black deep-sea fishes (shown by white circles) are well optimized to produce the lowest reflectances. Melanosomes from the skin of other ectothermic vertebrates (n = 50 species; gray triangles) are smaller for their aspect ratio than those of deep-sea fish and, according to our model, would produce higher reflectances [8, 10–18]. Melanosome sizes between 600 nm and 800 nm and aspect ratios between 1.5 and 3.0 produce the lowest reflectance, and all but two species of ultra-black deep-sea fish fall within this range. Gray contours represent reflectance values of 1.5%, 3%, 5%, and 10%. Point sizes are scaled so the area of the point is proportional to the median measured reflectance of that species.

(B) Melanosome size (as sphere equivalent diameter) for seven species of ultra-black fishes (black lines indicate median value).

(C) Melanosome aspect ratio for the same seven species (black lines indicate median value).

indicates that, due to differences in melanosome geometry, even if other ectothermic vertebrates had continuous melanosome layers, those layers would produce higher reflectances than the fishes studied here. These differences between ultra-black fishes and other ectothermic vertebrates suggest that melanosome geometry observed in deep-sea fishes is not typical of ectothermic vertebrates and may have evolved to minimize reflectance. Additionally, the relationship between melanosome geometry and reflectance may be important in generating variation in melanin-based coloration in other vertebrate taxa.

Effect of Melanosome Layer Thickness

Although most of the ultra-black species we examined via SEM had melanosomes with geometries that predict low reflectance in our models, the blackest species measured (*Oneirodes* sp.) is predicted to have a higher reflectance than other species analyzed here. This poor agreement between the modeled and measured reflectance of *Oneirodes* sp. may be a result of modeling melanosome layers with the same thickness for all combinations of melanosome SED and aspect ratio. *Oneirodes* sp. has the thickest layer of melanosomes, indicating that the thickness of the melanosome layer may influence reflectance. To investigate the effect of layer thickness on reflectance, we performed 10 additional simulations in which we varied the thickness of the melanosome layer between 1 μm and 10 μm with the same 5 × 5 μm cross section as the previous simulations, using melanosomes with SED = 800 nm and an aspect ratio of 2.0 (the combination of SED and aspect ratio with the lowest modeled reflectance). Reflectance decreased from 9.1% with a 1-μm-thick layer to 3.6% reflectance with a 2-μm layer to 2.0% reflectance for a 3-μm layer (Figure 4A, grey dots). The predicted reflectance averaged across 400–700 nm was roughly constant once the layer was thicker than 7 μm. Typically, when a material is neither optically thick (i.e., changing the thickness of the material does not change its reflectance) nor strongly reflective at its surface, a doubling of the thickness results in reflectance that is the square of the original reflectance (when reflectance is treated as a fraction). In our simulations varying melanosome layer thickness, we find that the reflectance does not decrease with increasing thickness as quickly as that relationship would predict (Figure 4A, black curve). Therefore, reflectance from the skin of black fishes is likely to be significantly affected by surface reflection from the top of the layer.

Effect of Reflectance on Underwater Sighting Distance

We have demonstrated that at least 16 species of deep-sea fish reflect less than 0.5% of perpendicularly incident light at 480 nm, making them some of the blackest known animals. Ultra-black coloration is achieved with a continuous, thin layer of melanosomes that are optimized in size and aspect ratio to produce the lowest reflectance. It is unclear, however, the magnitude of camouflage benefits conferred by being ultra-black as opposed to just black. To determine the camouflage benefits of ultra-black skin, we used a computational model developed by Ruxton and Johnsen [42] to calculate the relative sighting distances by predators of fishes with skin reflectance ranging from 2% to 0% (where the sighting distance would equal zero on perfectly black background). We calculate relative sighting distances (as opposed to absolute distances) because without knowing the intensity of a light source of the shape of the beam, absolute values are unlikely to be accurate. At low light levels, as is the case with a fish

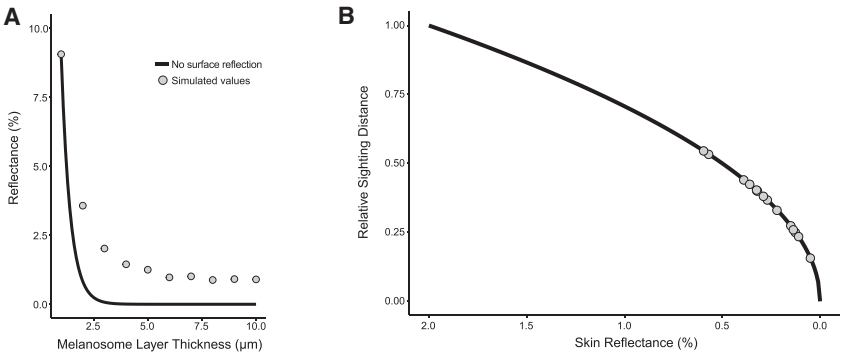

Figure 4. Effect of Layer Thickness and Camouflage Benefit of Ultra-black Skin

(A) Comparison of predicted reflectance for a material that is not optically thick or limited by surface reflection and simulated reflectance from melanosome aggregations varying in thickness from 1 μm to 10 μm. This suggests that the reflectance from melanosome layers is significantly limited by reflection from the surface, not by the absorption of the layer. The melanosomes in these simulations had an aspect ratio of 2.0 and SED of 800 nm (approximately the combination producing the lowest reflectance).

(B) Reducing skin reflectance from the maximum to the minimum measured here—2%–0.05%, that of *Oneirodes* sp.—decreases the relative sighting distance of the fish by 6-fold. Points along the line represent individual species. For computational model of sighting distance, see STAR Methods.

reflecting <2% of an already dim source (i.e., a bioluminescent flash, lure, glow, or searchlight), against the black deep-sea background, the model predicts that the sighting distance is proportional to the square root of the number of photons being reflected back to the viewer. Using this relationship, we find that reducing skin reflectance from 2% to 1% reduces sighting distance by 29% and that decreasing further to 0.5% or 0.05% reflectance reduces sighting distance by 50% and 84%, respectively (Figure 4). Because visual predators typically search a volume of space, and this reduction in sighting distance is linear, the camouflage benefits of ultra-black skin may be even greater than the reduction in sighting distance calculated here. Given the small size of the fishes studied here, it is likely that predator-prey interactions occur over short distances, where even small differences in sighting distance can have meaningful effects on interaction outcomes.

In most described ultra-black taxa (e.g., birds, butterflies, and jumping spiders), black patches are bordered by brightly colored patches, and adjacent areas of bright coloration and very low reflectance are thought to increase the contrast of color signals [31–33]. Here, we propose a different function of ultra-black coloration—camouflage (as has been proposed for the structurally enhanced black coloration in vipers [43] and stick insects [44]). The mechanism we describe here that underlies extremely low reflectance in deep-sea fishes—absorption by melanin in a highly scattering architecture—is similar to those found in birds, butterflies, and jumping spiders [31–33]. However, in fishes, the light scattering is caused by the melanosomes themselves without the need for the chitin or keratin matrices present in other taxa [31–33, 45]. This simple arrangement of close-packed, small particles with a size and shape optimized to produce the lowest reflectance has the potential to inspire the development of new synthetic ultra-black materials.

STAR★METHODS

Detailed methods are provided in the online version of this paper and include the following:

SUPPLEMENTAL INFORMATION

Supplemental Information can be found online at https://doi.org/10.1016/j.cub.2020.06.044.

ACKNOWLEDGMENTS

We thank Kakani Katija and MBARI's Bioinspiration Group for invitations to K.J.O., S.J., and K.N.T. to participate in an R/V *Western Flyer* expedition, where many of the spectrometry measurements were made. We also thank the captains, crews, and pilots of the R/V *Point Sur*, R/V *Western Flyer*, and ROV *Doc Ricketts* for their skills and dedication to deep ocean exploration; Jesse Granger, Sarah Solie, and Drs. Eleanor Caves and Carlos Taboada for helpful comments on an earlier version of the manuscript; Michelle Plue for assistance with TEM; Scott Whittacker for SEM tissue preparation protocols; Drs. William Kier and Laura Bagge for consulting on histological results and assisting with imaging; and Sancy Leachman for the invitation to participate in the 2018 Montagna Biology of the Melanocyte conference. Josh Havassy measured melanin granules. Christine Brantner provided technical assistance at George Washington University Transmission Electron Microscopy Lab. Anela Choy and Dr. Tracey Sutton provided fish identifications. Kyra Schlining, Rob Sherlock, Kim Reisenbichler, Stephanie Bush, Lynne Christianson, Shannon Johnson, and Joost Daniels provided logistical support and shipboard assistance. Funding for this work was provided from a NOAA Ocean Exploration and Research grant (NA17OAR0110208) to S.J., as well as the Biology Department at Duke University. A.L.D. conducted this research with government support under and awarded by the DOD, Army Research Office, National Defense Science and Engineering Graduate Fellowship (NDSEG). K.J.O. and F.E.G. were funded by the Smithsonian National Museum of Natural History.

AUTHOR CONTRIBUTIONS

A.L.D. contributed concept, spectrophotometry, microscopy, optical modeling, writing, specimen collection, and editing. K.N.T. contributed

spectrophotometry, editing, and specimen collection. F.E.G. contributed light and TEM histology. B.H.R. contributed access to specimens, fish identification, and editing. S.J. contributed concept, spectrophotometry, specimen collection, writing, and editing. K.J.O. contributed concept, microscopy, specimen collection, writing, and editing.

DECLARATION OF INTERESTS

The authors declare no competing interests.

Received: April 28, 2020
Revised: May 25, 2020
Accepted: June 12, 2020
Published: July 16, 2020

REFERENCES

1. Haddock, S.H., Moline, M.A., and Case, J.F. (2010). Bioluminescence in the sea. Annu. Rev. Mar. Sci. *2*, 443–493.
2. Widder, E.A. (2010). Bioluminescence in the ocean: origins of biological, chemical, and ecological diversity. Science *328*, 704–708.
3. Young, R.E. (1983). Oceanic bioluminescence: an overview of general functions. Bull. Mar. Sci. *33*, 829–845.
4. Martini, S., and Haddock, S.H. (2017). Quantification of bioluminescence from the surface to the deep sea demonstrates its predominance as an ecological trait. Sci. Rep. *7*, 45750.
5. Johnsen, S. (2005). The red and the black: bioluminescence and the color of animals in the deep sea. Integr. Comp. Biol. *45*, 234–246.
6. Zylinski, S., and Johnsen, S. (2011). Mesopelagic cephalopods switch between transparency and pigmentation to optimize camouflage in the deep. Curr. Biol. *21*, 1937–1941.
7. Hawkes, J.W. (1974). The structure of fish skin. I. General organization. Cell Tissue Res. *149*, 147–158.
8. Le Guellec, D., Morvan-Dubois, G., and Sire, J.-Y. (2004). Skin development in bony fish with particular emphasis on collagen deposition in the dermis of the zebrafish (*Danio rerio*). Int. J. Dev. Biol. *48*, 217–231.
9. Beeching, S.C., Glass, B.A., and Rehorek, S.J. (2013). Histology of melanic flank and opercular color pattern elements in the Firemouth Cichlid, *Thorichthys meeki*. J. Morphol. *274*, 743–749.
10. Burton, D. (1978). Melanophore distribution within the integumentary tissues of two teleost species, *Pseudopleuronectes americanus* and *Gasterosteus aculeatus* form *leiurus*. Can. J. Zool. *56*, 526–535.
11. Djurdjevič, I., Kreft, M.E., and Sušnik Bajec, S. (2015). Comparison of pigment cell ultrastructure and organisation in the dermis of marble trout and brown trout, and first description of erythrophore ultrastructure in salmonids. J. Anat. *227*, 583–595.
12. Faílde, L.D., Bermúdez, R., Vigliano, F., Coscelli, G.A., and Quiroga, M.I. (2014). Morphological, immunohistochemical and ultrastructural characterization of the skin of turbot (*Psetta maxima* L.). Tissue Cell *46*, 334–342.
13. Park, J.Y. (2002). Structure of the skin of an air-breathing mudskipper, *Periophthalmus magnuspinnatus*. J. Fish Biol. *60*, 1543–1550.
14. Guo, H., Huang, B., Qi, F., and Zhang, S. (2007). Distribution and ultrastructure of pigment cells in the skins of normal and albino adult turbot, *Scophthalmus maximus*. Chin. J. Ocean. Limn. *25*, 199–208.
15. Hirata, M., Nakamura, K., and Kondo, S. (2005). Pigment cell distributions in different tissues of the zebrafish, with special reference to the striped pigment pattern. Dev. Dyn. *234*, 293–300.
16. Hirose, E., and Matsumoto, J. (1993). Deficiency of the gene B impairs differentiation of melanophores in the medaka fish, *Oryzias latipes*: fine structure studies. Pigment Cell Res. *6*, 45–51.
17. Li, Q., Clarke, J.A., Gao, K.Q., Zhou, C.F., Meng, Q., Li, D., D'Alba, L., and Shawkey, M.D. (2014). Melanosome evolution indicates a key physiological shift within feathered dinosaurs. Nature *507*, 350–353.
18. Nakamura, N., Ikeda, Y., and Obika, M. (1987). Video and electron microscopic studies on pigment transport in *Gambusia* melanophores. Jap. J. Ichth. *34*, 351–360.
19. Obika, M., and Meyer-Rochow, V.B. (1990). Dermal and epidermal chromatophores of the Antarctic teleost Trematomus bernacchii. Pigment Cell Res. *3*, 33–37.
20. Rossi, V., McNamara, M.E., Webb, S.M., Ito, S., and Wakamatsu, K. (2019). Tissue-specific geometry and chemistry of modern and fossilized melanosomes reveal internal anatomy of extinct vertebrates. Proc. Natl. Acad. Sci. USA *116*, 17880–17889.
21. Sköld, H.N., Aspengren, S., and Wallin, M. (2002). The cytoskeleton in fish melanophore melanosome positioning. Microsc. Res. Tech. *58*, 464–469.
22. Johnsen, S. (2014). Hide and seek in the open sea: pelagic camouflage and visual countermeasures. Annu. Rev. Mar. Sci. *6*, 369–392.
23. McFall-Ngai, M.J. (1990). Crypsis in the pelagic environment. Am. Zool. *30*, 175–188.
24. Herring, P.J. (1977). Bioluminescence of marine organisms. Nature *267*, 788–793.
25. Widder, E.A. (1999). Bioluminescence. In Adaptive Mechanisms in the Ecology of Vision, S.N. Archer, M.B.A. Djamgoz, E.R. Loew, J.C. Partridge, and S. Vallerga, eds. (Kluwer Academic), pp. 555–581.
26. Young, R.E., Kampa, E.M., Maynard, S.D., Mencher, F.M., and Roper, C.F.E. (1980). Counterillumination and the upper depth limits of midwater animals. Deep Sea Res. A. *27*, 671–691.
27. Johnsen, S. (2001). Hidden in plain sight: the ecology and physiology of organismal transparency. Biol. Bull. *201*, 301–318.
28. Johnsen, S. (2003). Lifting the cloak of invisibility: the effects of changing optical conditions on pelagic crypsis. Integr. Comp. Biol. *43*, 580–590.
29. Childress, J.J., Barnes, A.T., Quetin, L.B., and Robison, B.H. (1978). Thermally protecting cod ends for the recovery of living deep-sea animals. Deep Sea Res. *25*, 419–422.
30. Widder, E.A., Latz, M.I., and Case, J.F. (1983). Marine bioluminescence spectra measured with an optical multichannel detection system. Biol. Bull. *165*, 791–810.
31. Davis, A.L., Nijhout, H.F., and Johnsen, S. (2020). Diverse nanostructures underlie thin ultra-black scales in butterflies. Nat. Commun. *11*, 1294.
32. McCoy, D.E., Feo, T., Harvey, T.A., and Prum, R.O. (2018). Structural absorption by barbule microstructures of super black bird of paradise feathers. Nat. Commun. *9*, 1–8.
33. McCoy, D.E., McCoy, V.E., Mandsberg, N.K., Shneidman, A.V., Aizenberg, J., Prum, R.O., and Haig, D. (2019). Structurally assisted super black in colourful peacock spiders. Proc. Biol. Sci. *286*, 20190589.
34. Mizuno, K., Ishii, J., Kishida, H., Hayamizu, Y., Yasuda, S., Futaba, D.N., Yumura, M., and Hata, K. (2009). A black body absorber from vertically aligned single-walled carbon nanotubes. Proc. Natl. Acad. Sci. USA *106*, 6044–6047.
35. Kumar, S., Stecher, G., Suleski, M., and Hedges, S.B. (2017). TimeTree: a resource for timelines, timetrees, and divergence times. Mol. Biol. Evol. *34*, 1812–1819.
36. Robison, B.H., Ruby, E.G., and Morin, J.G. (1977). Luminous bacteria associated with the gut contents of midwater fishes. West. Soc. Nat. *58*, 23.
37. Ruby, E.G., and Morin, J.G. (1979). Luminous enteric bacteria of marine fishes: a study of their distribution, densities, and dispersion. Appl. Environ. Microbiol. *38*, 406–411.
38. Goda, M., and Fujii, R. (2001). Coloration and chromatophores of the domino damsel, *Dascyllus trimaculatus*. Zool. Sci. *18*, 165–174.
39. Hawkes, J.W. (1974). The structure of fish skin. II. The chromatophore unit. Cell Tissue Res. *149*, 159–172.
40. Kalogianni, E., Alexis, M., Tsangaris, C., Abraham, M., Wendelaar Bonga, S.E., Iger, Y., van Ham, E.H., and Stoumboudi, M.T. (2011). Cellular responses in the skin of the gilthead sea bream *Sparus aurata* L. and the sea bass *Dicentrarchus labrax* (L.) exposed to high ammonia. J. Fish Biol. *78*, 1152–1169.

41. Roberts, R.J., Young, H., and Milne, J.A. (1972). Studies on the skin of plaice (*Pleuronectes platessa* L.) 1. The structure and ultrastructure of normal plaice skin. J. Fish Biol. *4*, 87–98.

42. Ruxton, G.D., and Johnsen, S. (2016). The effect of aggregation on visibility in open water. Proc. Biol. Sci. *283*, 20161463.

43. Spinner, M., Kovalev, A., Gorb, S.N., and Westhoff, G. (2013). Snake velvet black: hierarchical micro- and nanostructure enhances dark colouration in *Bitis rhinoceros*. Sci. Rep. *3*, 1846.

44. Maurer, D.L., Kohl, T., and Gebhardt, M.J. (2017). Cuticular microstructures turn specular black into matt black in a stick insect. Arthropod Struct. Dev. *46*, 147–155.

45. Wong, V.L., and Marek, P.E. (2020). Structure and pigment make the eyed elater's eyespots black. PeerJ *8*, e8161.

46. Bagge, L.E., Osborn, K.J., and Johnsen, S. (2016). Nanostructures and monolayers of spheres reduce surface reflections in hyperiid amphipods. Curr. Biol. *26*, 3071–3076.

47. Spurr, A.R. (1969). A low-viscosity epoxy resin embedding medium for electron microscopy. J. Ultrastruct. Res. *26*, 31–43.

48. Richardson, K.C., Jarett, L., and Finke, E.H. (1960). Embedding in epoxy resins for ultrathin sectioning in electron microscopy. Stain Technol. *35*, 313–323.

49. Schindelin, J., Arganda-Carreras, I., Frise, E., Kaynig, V., Longair, M., Pietzsch, T., Preibisch, S., Rueden, C., Saalfeld, S., Schmid, B., et al. (2012). Fiji: an open-source platform for biological-image analysis. Nat. Methods *9*, 676–682.

50. R Development Core Team (2014). R: A language and environment for statistical computing (R Foundation for Statistical Computing). http://www.R-project.org/.

51. RStudio Team (2015). RStudio: Integrated Development for R (RStudio). http://www.rstudio.com/.

52. Stavenga, D.G., Leertouwer, H.L., Osorio, D.C., and Wilts, B.D. (2015). High refractive index of melanin in shiny occipital feathers of a bird of paradise. Light Sci. Appl. *4*, e243.

53. Johnsen, S., and Widder, E.A. (1999). The physical basis of transparency in biological tissue: ultrastructure and the minimization of light scattering. J. Theor. Biol. *199*, 181–198.

54. Jennings, B.R., and Parslow, K. (1988). Particle size measurement: the equivalent spherical diameter. Proc. R. Soc. Lond. A Math. Phys. Sci. *419*, 137–149.

STAR★METHODS

KEY RESOURCES TABLE

REAGENT or RESOURCE	SOURCE	IDENTIFIER
Biological Samples		
Deep-sea Fishes	Wild Caught	N/A
Deposited Data		
Mendeley	Online	https://doi.org/10.17632/6t6sw3mpy3.1
Software and Algorithms		
RStudio	Online (Free)	https://rstudio.com/
Lumerical	Online (License)	https://www.lumerical.com/
TimeTree	Online (Free)	http://www.timetree.org/
ImageJ (Fiji)	Online (Free)	https://imagej.nih.gov/ij/download.html

RESOURCE AVAILABILITY

Lead Contact

Further information and requests for resources should be directed to and will be fulfilled by the Lead Contact, Alexander L. Davis (alexander96davis@gmail.com).

Materials availability

This study did not generate any unique reagents.

Data and Code Availability

Supporting data for this manuscript can be found in Mendeley Data (https://doi.org/10.17632/6t6sw3mpy3.1)

EXPERIMENTAL MODEL AND SUBJECT DETAILS

We focused our sampling efforts on mesopelagic and bathypelagic fishes that typically occupy depths where ambient sunlight levels are below the thresholds of vision. Specimens for histology were collected on multiple R/V *Western Flyer* research cruises from April 2014 to June 2018 and one research cruise on the R/V *Point Sur* in the Gulf of Mexico in June 2019. In total, we measured reflectance of 39 meso- and bathypelagic fish specimens from 18 species on two research cruises, the first in the Monterey Bay, CA (R/V *Western Flyer*) and the second in the Gulf of Mexico (R/V *Point Sur*) (Gulf of Mexico: 8-22 June 2019, Lat: ~27.5°N Long: ~87°W; Monterey Bay: 21-26 June 2018, Lat: ~36.7°N Long: ~122°W; Table S1). Specimens were collected via Tucker trawl between 0 m and 2000 m [29] or with the remotely operated vehicle *Doc Ricketts*. Most specimens were dead or moribund, but, immediately after collection, specimens were placed in chilled seawater (4-6°C) to minimize tissue degradation until reflectance measurements. Measurements were taken within one hour of specimen recovery. Tissue samples were taken following reflectance measurements.

METHOD DETAILS

Reflectance measurements

Many deep-sea, pelagic fishes have delicate skin, which makes damage from the trawl net common. We chose specimens for our reflectance measurements that had either fully intact skin or large areas of intact skin with minimal visible damage. It is possible that there was damage to the epidermis of our specimens from the net, however, given how thin the epidermis is and that it is generally transparent in fishes, it is likely that any error caused by this damage would act to increase our measured reflectance (therefore providing an underestimate of how black these fishes are). This damage to the epidermis may also have prevented us from evaluating the presence of other modifications to tissue ultrastructure that could minimize surface reflection (i.e., antireflection coatings that have been found in some deep-sea amphipods [46]). Spectral reflectance was measured from freshly-caught fish in seawater using a multi-channel spectroradiometer (USB2000 Ocean Optics Inc., Dunedin, FL, USA) coupled with a Xenon UV-VIS light source (PX-2 Ocean Optics) and fiber-optic back-reflectance probe (R400-7 Ocean Optics) run through OceanView acquisition software (v.1.6.7). We took measurements at 90° relative to the plane of the skin. The skin reflectance was measured from 3-6 locations per specimen depending on the amount of undamaged skin and the size of the fish (the number of measurements per species can be found in Table S1). Following Davis et al. [31], all measurements were calibrated to a Spectralon™ block with 2% diffuse reflectance (Labsphere, North Sutton, NH, USA) and then divided by 50 to get the reflectance relative to a 100% white standard. We report the median reflectance across all measurements for a species, as opposed to average reflectance from these measurements, because the reflectance

values are so small that just a single relatively high reflectance measurement (from a slightly damaged area of skin, for example) can skew the average reflectance (for individual reflectance spectra see Figure S1).

Histological analysis

We performed histology on samples of skin from 15 species of fishes from eight distantly related orders (Table S1). Specimens were prepared in two labs with similar but varying protocols. Differences in specimen preparation are not likely to substantially affect the results because melanosomes are structurally robust. Below are the methods pertaining to each species. *Oneirodes* sp. (Figures 2A and S2E), *Photostomias guernei* (Figure S2M), *Bassozetus compressus, Echiostoma barbatum* (juvenile, Figures S2K and S2L), *Eurypharynx pelecanoides* (Figure S2A), *Eustomias schmidti, Lampadena luminosa,* and *Pseudoscopelus* sp. were prepared as follows. Small sections of skin were placed in 2.5% glutaraldehyde buffered with seawater for light microscopy and scanning and transmission electron microscopy (SEM and TEM, respectively). For TEM, small pieces of skin were cut using a razor blade, washed with 1x phosphate-buffered saline (PBS), post-fixed with 1% osmium tetroxide (OsO_4), then stained with 0.5% uranyl acetate. Following staining, the samples were placed in 30% ethanol and dehydrated to 100% ethanol in a stepwise fashion. Once the samples were fully dehydrated, they were embedded in Spurr's resin [47], sectioned using a diamond knife on a Leica Ultracut microtome (Leica, Wetzlar, Germany), and collected on copper TEM grids. The grids were then imaged at the Duke Shared Materials and Instrumentation Facility on an FEI Tecnai G^2 Twin transmission electron microscope (ThermoFisher Scientific, Waltham, MA, USA) at magnifications between 1700x – 19000x. Samples for SEM were dehydrated in the same process as TEM samples, then dried using a LADD CPD3 critical point dryer (Ladd Research Industries, Williston, VT, USA) to preserve tissue ultrastructure. Specimens were then mounted on aluminum SEM stubs using copper tape and sputter coated with ~7nm of gold (Denton Desk V; Denton Vacuum LLC, Moorestown, NJ, USA). The samples were imaged using an Apreo S scanning electron microscope (ThermoFisher Scientific, Waltham, MA, USA) at the Duke Shared Materials and Instrumentation Facility with an acceleration voltage of 1kV and magnifications between 1200x – 6500x. Finally, slides for light-level histology were generated by taking thin sections in the same manner as TEM and staining them with Toluidine blue, mounting them with coverslips, and imaging them on a Zeiss Axiocam HRc digital camera on a Zeiss Axiophot microscope (Zeiss, Oberkochen, Germany).

Anoplogaster cornuta, Cetominus sp., Cyclothone sp. (Figures S2I and S2J), Idiacanthus antrostomus (Figures 2B–2F and S2N–S2Q), Lampanyctus sp. (Figures S2F and S2G), Poromitra crassiceps (Figures S2B–S2D), Sagamichthyes abei (Figure S2H), and Stomias sp. were prepared using the following methods. Intact skin, typically the ventral surface or behind the pectoral fins, was excised from specimens then fixed in either 2% cacodylate buffered glutaraldehyde or 4% formaldehyde in seawater. Tissues for SEM were transferred to hexamethyldisilazane through a dehydration series and dried overnight in a fume hood before mounting and coating with gold-palladium for examination with a Zeiss EVO MA 15 scanning electron microscope at the Smithsonian National Museum of Natural History (NMNH) Scientific Imaging Lab. Tissues for light microscopy and TEM were embedded Spurr's Low-Viscosity resin [47] from Polysciences, Hardness A prior to sectioning and staining. Thick sections for light microscopy and ultra-thin sections for TEM were sectioned with the RMC MT6000 ultramicrotome, thick (1 μm) with the Histo Jumbo diamond knife (Diatome, US) and ultra-thin (70 and 100 nm) with a 45° diamond knife (DuPont Instruments). Thick sections were mounted either unstained or stained with Richardson's blue [48] prior to imaging with an Olympus BX63F Compound Fluorescent Microscope (Olympus Corporation, Tokyo, Japan) at the NMNH Scientific Imaging Lab. Ultrathin sections were collected on copper grids and stained for TEM with 2% uranyl acetate in 50% ethanol and 0.4% lead citrate in basic water (1 sodium hydroxide pellet per 50 mL water). Grids were imaged with the FEI Talos F200X TEM at George Washington University Nanofabrication and Imaging Center.

We used SEM to analyze melanosome geometry. We were able to visualize the melanosomes by imaging the side of the skin that was cut by the razor blade or in areas where we had disrupted the epidermal basement membrane. We then used Fiji [49] to measure the short and long axes of 40-100 individual melanosomes per species to calculate the aspect ratio and sphere equivalent diameter (SED). We also used Fiji [49] for analysis of light microscopy images to measure the thickness of the melanosome layer at 30 evenly spaced locations along one section of skin per species. All calculations were done using R [version 3.6.2] via RStudio [version 1.2.5033] [50, 51].

Comparing melanosome geometry to published values

In order to assess the possibility that melanosomes in deep-sea fishes are specialized to produce low reflectance, we compared the geometric parameters calculated here (SED and AR) to previously published data on melanosome geometry from the skin of ectothermic vertebrates. We limited our comparison to ectothermic vertebrates because mammals and birds have changes in melanosome morphology associated with metabolism [17]. Additionally, we only considered melanosomes in the skin because melanosome geometry is known to vary by tissue type [20]. In total, we assessed melanosome geometry in 50 species across reptiles, amphibians, and fishes. Thirty-six species were drawn from Li et al. [17], six from Rossi et al. [20], and the remaining eight were measured from published TEM images of fish melanophores [9, 11–14, 18, 19]. Melanosome measurements were taken from TEM images using Fiji [46]. Because measurements from TEM images are biased toward small sizes, as the plane through which the melanosome was cut is not known, we report the maximum measured SED from available images and the corresponding aspect ratio, in Figure 3.

Optical modeling

To assess the effect of melanosome geometry on reflectance, we performed three-dimensional finite-difference time-domain (FDTD) simulations of random closed-packed ellipsoids using the Lumerical FDTD solver version 2019b (Lumerical Inc.,Vancouver, BC,

Canada)). In FDTD simulations, Maxwell's equations are solved across a three-dimensional grid with a user-specified resolution, and the electromagnetic waves evolving iteratively through time. Random close-packed aggregations of ellipsoids mimicking the arrangement seen in the dermis of deep-sea fishes were generated by modifying the Uniform Random Particle Distribution (URPD) structure in Lumerical to include a term for the aspect ratio of the melanosome and specify random angles of orientation in the x, y, and z-plane. Generally, the URPD structure generates an array of non-overlapping objects until either the domain has been filled or the desired maximum number of objects have been added. Then, the function repeats this process a specified number of times to maximize the number of objects. In our case, the object was an ellipsoid made of melanin and we set the number of iterations of the function to 2000. The desired number of ellipsoids was set to be greater than the maximum number that would fit in the domain to ensure close packing.

After modifying the URPD structure to generate ellipsoids of different aspect ratios, we simulated 169 combinations of melanosome aspect ratio and sphere equivalent diameter (SED) by varying the aspect ratio from 1.0 to 4.0 in increments of 0.25 and SED from 100nm to 3000nm (100nm intervals for SED $\leq$ 1000nm and 500nm intervals for SED > 1000). For these simulations, we used a minimum mesh step of 0.25nm, a 5μm x 5μm x 5μm domain (except for SED = 100nm and 200nm which had the same thickness as the other simulations but due to computational constraints had cross sections of 1μm x 1μm and 2μm x 2μm, respectively). All simulations had periodic boundary conditions in the x and y directions, a plane wave source (400nm – 700nm) propagating in the z direction, and a reflecting boundary condition backing the melanosome layer to approximate reflective collagen and muscle tissue underneath the melanosomes. The real part of the refractive index of the melanosomes was set by the Cauchy equation, $n(\lambda) = A + B/\lambda^2$ where $A = 1.648$ and $B = 2.37 \times 10^4\ nm^2$, and the imaginary part of the refractive index was fitted with the exponential $k(\lambda) = 0.56e^{-\lambda/270nm}$ [52] (Figure S3). The melanosomes were assumed to be embedded in a medium with a uniform refractive index of $n = 1.33$, closely approximating those of seawater and cytoplasm [53].

To determine the effect of melanosome layer thickness on reflectance, we performed 10 additional simulations varying the thickness of the domain from 1μm to 10μm in 1μm intervals. All 10 simulations were performed with 800nm melanosomes that had an aspect ratio of 2.0 (approximately the combination that produced the lowest reflectance in our model).

Sighting Distance Calculation

To calculate the benefit of reduced skin reflectance, we used the computational sighting distance model from Ruxton and Johnsen [42] to calculate relative sighting distances of fishes with skin reflectance ranging from 0% to 2%. In this model the sighting distance is proportional to the LambertW function of the square root of the number of photons leaving the target (where the LambertW function is the inverse of $y = xe^x$). Because the fish is reflecting < 2% of the photons from an already dim source (a bioluminescent searchlight, flash, or glow), the LambertW is roughly linear and the relative sighting distance depends on the square root of the number of photons being reflected back by the fish. Normalized values were used because the beam shape emitted from the bioluminescence of deep-sea animals is unknown and it undoubtedly varies from species to species. Without knowing the beam shape, it is not possible to determine what percentage of emitted photons hit the prey fish and any absolute sighting distance values are likely to be incorrect. We took the relative sighting distance to be 1.0 at a reflectance of 2%, then fit a square root function that travels through the origin and 1.0 at 2% to calculate relative sighting distance for reflectances between 0% and 2% ($r = (\sqrt{Reflectance}/\sqrt{2})$).

QUANTIFICATION AND STATISTICAL ANALYSIS

Reflectance spectra

All reflectance spectra were imported into RStudio [51] and then normalized to a calibration standard with 100% reflectance (all values were initially recorded relative to a 2% reflectance standard). The reflectance at 480nm reported in Figure 1 was calculated as the median reflectance at 480nm across all measurements for a given species. We then fit a LOESS regression for each species in RStudio to the median reflectance at every wavelength (Figure S1). The average reflectance from 350-700nm for each species is reported as the area under the LOESS curve divided by the wavelength range (350nm).

Melanosome geometry

We calculated the mean and median melanosome aspect ratio from between 40 and 100 individual melanosomes per species in RStudio (exact number of melanosomes for each species can be found in Figure 3). All melanosome sizes are reported as the melanosome sphere equivalent diameter (SED). For the purposes of calculating SED melanosomes were treated as prolate ellipsoids and SED is given by the expression $(d_l/r^{2/3})$, where d_l is the length of the long axis of the melanosome and r is the ratio of the long axis to the short axis [54].

FDTD Simulations

FDTD simulations of reflectance from close-packed melanosomes yielded reflectance values for wavelengths between 400-700nm. We then calculated the mean reflectance from 400-700nm for every combination of melanosome aspect ratio and sphere equivalent diameter (n = 169 simulations). After calculating the average reflectance for each simulation we used LOESS regression to interpolate reflectance for combinations of aspect ratio and SED within our simulated range (Figure 3A).